photonics

MDPI

Article

Scattering Characteristics of Gaussian Vortex Beams in Aerosol-Laden Atmosphere for Communication Systems and Multimedia Information Transmission

Bader Alhasson [1], Faroq Razzaz [1,2] and Muhammad Arfan [3,4,*]

[1] Department of Electrical Engineering, College of Engineering in Al-Kharj, Prince Sattam Bin Abdulaziz University, Al-Kharj 16242, Saudi Arabia
[2] Faculty of Engineering and Information Technology, Taiz University, Taiz 6803, Yemen
[3] School of Sciences, Department of Physics, School Education Department, Government of Punjab, Faisalabad 38000, Pakistan
[4] Department of Physics, University of Agriculture, Faisalabad 38000, Pakistan
* Correspondence: marfan9358@gmail.com

Abstract

The interaction of electromagnetic waves with atmospheric aerosols plays a significant role in communication systems and multimedia information transmission. Understanding the interaction of vortex light beams with an aerosol-laden atmosphere is indispensable for establishing a framework of the environmental channel. During the interaction, different optical effects such as absorption and scattering will result in energy attenuation, and this yields the deterioration of the transmission feature of the vortex beam signal. In this study, we present a theoretical analysis of Gaussian vortex beams (GVBs) scattering by diverse aerosol (unformed carbon, dust, sulphate, silicate, soot, and nitrate) particles in the atmosphere on the basis of the well-established generalized Lorenz–Mie theory (GLMT). Combined with the lognormal distribution model for aerosol particles, the attenuation and transmission characteristics of GVBs for different aerosol particles are analyzed. The extinction efficiency (Q_{ext}) factor of GVB, caused by the absorption and scattering of various aerosols, becomes smaller compared to that of a basic Gaussian beam (GB). Increasing the OAM mode index, the energy attenuation and transmission caused by aerosol absorption and scattering further decrease. Moreover, this research provides a basis to analyze the optical characteristics of the twisted beams in different atmospheric channels, such as wireless communication networks over aerosol-laden systems and material interactions.

Keywords: scattering; aerosol; communication; Gaussian vortex beam; attenuation

Check for updates

Received: 19 May 2026
Revised: 16 June 2026
Accepted: 22 June 2026
Published: 24 June 2026

Copyright: © 2026 by the authors. Licensee MDPI, Basel, Switzerland. This article is an open access article distributed under the terms and conditions of the Creative Commons Attribution (CC BY) license.

1. Introduction

Since the breakthrough following Allen et al.'s 1992 discovery of orbital angular momentum (OAM) [1], which developed a link between OAM and vortex beams, these beams have attracted significant attention from the optical research community. Their unique spatial structure has potential applications in electromagnetics and optics, quantum physics, optical diagnostics, light manipulation, OAM imaging, wireless communication, material characterization, and many others, which are in turn boosting continued technological developments [2–4]. Vortex beams, with their OAM and unique twisted phase profile, have unlocked a new era in laser and shaped beam technology, pushing the frontiers of technological progress [5]. The OAM of vortex beams makes them suitable candidates for

optical studies. Consequently, these beams are compatible with electromagnetic scattering analysis because of their ability to reduce interference effects.

Gaussian vortex beams (GVBs) are well-known due to their exciting applications [6,7]. Compared to basic Gaussian beams, which do not possess OAM, GVBs carry discrete OAM. The GVBs have potential usage in several domains, like optical guiding and trapping, medical imaging, optical engineering, and telecommunication [8]. The spiral wavefront profile of GVBs is indicated by an azimuthal phase dependence factor, $exp(il\varphi)$, where l symbolizes the topological charge or OAM mode index [9]. Unlike Gaussian beams, vortex beams show a ring-mode profile for intensity distribution with a dark central core whose radius scales along the optical axis with topological charge [10,11]. This redistribution of beam energy tunes the beam's interaction with scattering objects. Recent studies have proved that OAM remains conserved even following propagation through scattering biological media [12,13], exploring a topological resilience feature that proposes new avenues for exploiting vortex light beam scattering in complex optical channels.

Compared with basic Laguerre–Gaussian (LG) beams, GVBs preserve the helical phase profile and OAM. Besides that, GVBs also possess stronger spatial confinement of optical energy. The enhanced field localization can boost vortex-beam–particle interaction and impact the resulting scattering response. Furthermore, the flexibility in governing intensity distribution profile and beam width makes GVBs suitable for investigating scattering phenomena under focused-beam illumination. Consequently, the present study employs a GVB to analyze scattering dynamics of diverse spherical aerosol particles.

Recently, studies on aerosol particles have attracted the scientific community due to their broad impact on communication, optical ground stations, air quality, visibility, air traffic, and information technology [14–20]. The direct incorporation of communication technology into the routine activities of human beings makes it vulnerable to channel distortion caused by aerosol particles, which disrupts routine functions. Additionally, wireless communication is also limited by additional atmospheric effects, such as absorption, scattering, reflection, etc. The overall effect results in a degradation of the performance of the system [20,21]. The analysis of electromagnetic wave scattering and transmission in atmospheric aerosols is an essential route in characterizing communication signals, atmospheric radiation, signal propagation, monitoring remote sensing, climatic change, environmental tracking, and the efficiency of multimedia information transmission. Consequently, the transmission and scattering characteristics regarding vortex beams in complex aerosol scatterers will offer a theoretical framework for analyzing the aerosol dynamics.

The characteristics of vortex beams have been studied by the optical community. For free-space propagation, a vortex beam can encounter diverse objects, yielding information deterioration. The study investigates the phase retrieval of vortex beams [22]. It also addresses the decoding of OAM for free-space optical (FSO) communications. This work is added to highlight that phase retrieval is quite indispensable for investigating scattering characteristics of vortex beams in communication channels. Fractional vortex beams (FVBs) are well-known due to their distinguished optical characteristics and higher-dimensional OAM. The letter discusses the identification of fractional topological charges (TCs) [23]. It is noted that integer TCs generate vivid OAM states considering communication encoding, whereas fractional TCs (their focus) are more sensitive to scattering-mediated mode crosstalk.

The research presents a method to produce manageable OAM field distributions through grafted vortices [24]. The work is cited as a substitute approach for beam engineering, and it should be considered that our theoretical model of the GVB field is a special case of these types of structured beams. The review extensively embraces generation, beam shaping, propagation, OAM spectrum, and applications of FVBs [25]. The study is based

on fractional vortices, while our work focuses on integer-order GVBs in diverse aerosol scattering dynamics for communication systems.

Compared to those of prior published works, the present work focuses on systematic analysis of integer-order GVB scattering characteristics, considering various realistic spherical aerosol particles with full GLMT-dependent error quantification and communication network metrics.

The basic characterizing parameters, like particle size distribution, number density, and refractive index, may influence the scattering dynamics of aerosol particles. Fortunately, there are a number of analytical calculations and numerical results on these parameters in the published literature [26–29]. The absorption and scattering characteristics induced by aerosol particles result in the signal interruption and spreading of the OAM beam spectrum, which contribute towards distorting the signal quality [30]. The optical researchers are attracted to environmental optics, especially aerosols, due to their inclusion in human activities, including atmospheric variation and pollution, which significantly influence optical phenomena. Therefore, the study of characteristics of GVBs in complex environments becomes intriguing.

The researchers have analyzed the optical characteristics, i.e., propagation, trapping dynamics, transmission deterioration, and inversion techniques of different vortex beams in aerosol environments. In contrast, the present study focuses on the rigorous scattering characteristics of GVB by different spherical aerosol particles, where the dynamics of scattered fields are analyzed using a GLMT framework. The earlier published studies mainly focused on beam propagation over aerosol media [31,32], atmospheric transmission impacts [33], particle trapping [34], and aerosol characterization [35]; however, the present work deals extensively with scattering features of multiple aerosol particles illuminated by a GVB field, particularly within the present theoretical formulation, considering communication and multimedia information transmission, which are sufficiently explored.

Based on the GLMT [36,37], this work emphasizes the significance of efficiency factors for different aerosol particles irradiated by GVBs. Numerical results indicate that the scattering of higher-order GVBs by various aerosol particles is smaller compared to that of conventional Gaussian beams; this means propagation of GVBs in certain aerosol media has a higher optical transmission response when just analyzing the single scattering model.

Despite advancements in scattering research on GVBs, the interaction of GVBs with aerosol particles, and especially their scattering signatures, remains an unresolved gap. This gap is substantial because GVBs introduce tunable OAM states and twisting phase profiles that can influence both scattering dynamics and efficiency factors in ways not achievable with other shaped beams. Addressing this gap becomes important for atmospheric diagnostics and aerosol optics, where analytical modeling of both scattered intensity and efficiency factors is required. The research on the scattering and transmission characteristics of vortex beams by diverse aerosol particles in free space and the impacts on communication systems is still to be researched. This study also offers new theoretical insight into the interaction of twisted beams with different aerosol particles in the atmosphere and provides an avenue for further refinements in different communication channels and optical manipulation.

This work deals with the theoretical analysis of aerosol scattering dynamics on optical communication networks and multimedia information transmission over the extinction, scattering, absorption, attenuation, and transmittance characteristics of GVBs propagating in different aerosol-induced atmospheres using GLMT.

In this manuscript, a rigorous analytical theory regarding the scattering response of aerosol particles by GVBs is described. In the second section, the theory of scattering of GVBs using GLMT is presented. Besides this, the lognormal distribution model for aerosol particles is analyzed and discussed. Combined with the lognormal distribution model for

aerosol particles, the attenuation characteristics of GVB transmission in various atmospheric aerosols are also simulated. In the third section, the numerical results are presented and discussed. The last section embraces the conclusion for the proposed research.

2. Methods

The interaction of x-linearly polarized GVB propagating along the z-direction with a homogeneous spherical aerosol particle can be seen in Figure 1. The medium surrounding the aerosol particle is homogeneous, lossless, non-conducting, and non-magnetic. GVB is positioned in the coordinate system $OXYZ$ with its center O. For the spherical aerosol particle, the coordinates are taken as $oxyz$ with the center at o, respectively. Both coordinate systems are drawn as parallel to each other.

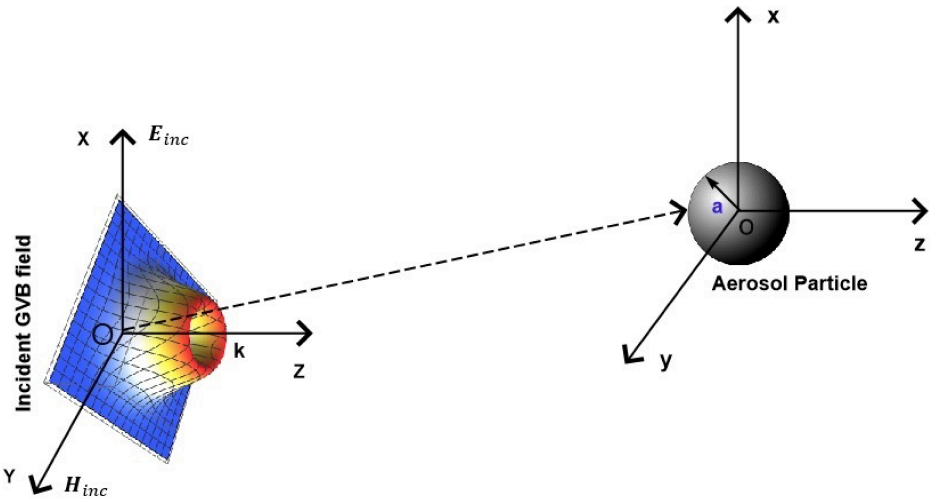


Figure 1. Geometry of the Interaction model of GVB with aerosol particle showing the incident electromagnetic fields $\boldsymbol{E}_{inc}$, $\boldsymbol{H}_{inc}$, and the target (spherical aerosol).

Based on the GLMT [36], the various types of electromagnetic fields, including incident, scattered, and internal, can be written as

$$\boldsymbol{E}^{inc} = \sum_{n=1}^{\infty}\sum_{m=-n}^{n} c_n^{pw}\left[g_{n,TM}^{m}\mathbf{N}_{mn}^{(1)} + ig_{n,TE}^{m}\mathbf{M}_{mn}^{(1)}\right] \tag{1}$$

$$\boldsymbol{H}^{inc} = \left(\frac{-ik}{\omega}\right)\sum_{n=1}^{\infty}\sum_{m=-n}^{n} c_n^{pw}\left[g_{n,TM}^{m}\mathbf{M}_{mn}^{(1)} + ig_{n,TE}^{m}\mathbf{N}_{mn}^{(1)}\right] \tag{2}$$

where $g_{n,TM}^{m}$ and $g_{n,TE}^{m}$ are known as beam shape coefficients (BSCs) and these govern the shape of the incident vortex beam field.

These can be given as [30]

$$g_{n,TM}^{m} = \begin{cases} \frac{-(-i)^{l+1}Z_n^m(w_0)^{l+2}(n+0.5)^l kz}{2^{(l+1)}(r^2+z^2)^{l/2+1}} e^{\left(\frac{-(w_0)^2}{4}\cdot\frac{(n+0.5)^2}{(r^2+z^2)}+ik(r^2+z^2)^{1/2}\right)} & m=-l\pm 1 \\ 0\ (otherwise) \end{cases} \tag{3}$$

$$g_{n,TE}^{m} = \begin{cases} \pm\left(\frac{(n+0.5)^2}{2k}-kz^2\right)\frac{(-i)^{l+2}Z_n^m(w_0)^{l+2}(n+0.5)^l}{2^{(l+1)}(r^2+z^2)^{l/2+1}} e^{\left(\frac{-(w_0)^2}{4}\cdot\frac{(n+0.5)^2}{(r^2+z^2)}+ik(r^2+z^2)^{1/2}\right)} & m=-l\pm 1 \\ \pm\frac{(-i)^{l+1}Z_n^m(w_0)^{l+2}(n+0.5)^{l+2}}{2^{(l+2)}(r^2+z^2)^{l/2+1}} e^{\left(\frac{-(w_0)^2}{4}\cdot\frac{(n+0.5)^2}{(r^2+z^2)}+ik(r^2+z^2)^{1/2}\right)} & m=-l\pm 3 \\ 0\ (otherwise) \end{cases} \tag{4}$$

Z_n^m characterize the normalization factor [36,38].

$$Z_n^{m=0} = \frac{2n(n+1)i}{2n+1} \tag{5}$$

$$Z_n^{m\neq 0} = \left(\frac{-2i}{2n+1}\right)^{|m|-1} \tag{6}$$

Here, n and m symbolize the degree and order of the vector spherical wave functions (VSWFs), respectively, and i = $\sqrt{-1}$. To normalize the BSCs used in the GLMT, the factor Z_n^m is introduced. Here, $\mathbf{M}_{mn}^{(1)}$ and $\mathbf{N}_{mn}^{(1)}$ denote the VSWFs, $k = \frac{\omega}{c} = \frac{2\pi}{\lambda}$ is the wave number phase constant, and ω is the angular frequency. Furthermore, $c_n^{pw} = i^n \frac{(n+0.5)}{n(n+1)}$, where the superscript pw designates the plane wave factor. The term l in Equations (3) and (4) denotes the OAM mode index or beam topological charge.

$$\boldsymbol{E}^{sca} = \sum_{n=1}^{\infty}\sum_{m=-n}^{n} c_n^{pw}\left[a_{mn}\mathbf{N}_{mn}^{(3)} + ib_{mn}\mathbf{M}_{mn}^{(3)}\right] \tag{7}$$

$$\boldsymbol{H}^{sca} = \left(\frac{-ik}{\omega}\right)\sum_{n=1}^{\infty}\sum_{m=-n}^{n} c_n^{pw}\left[a_{mn}\mathbf{M}_{mn}^{(3)} + ib_{mn}\mathbf{N}_{mn}^{(3)}\right] \tag{8}$$

$$\boldsymbol{E}^{int} = \sum_{n=1}^{\infty}\sum_{m=-n}^{n} c_n^{pw}\left[c_{mn}\mathbf{N}_{mn}^{(1)} + id_{mn}\mathbf{M}_{mn}^{(1)}\right] \tag{9}$$

$$\boldsymbol{H}^{int} = \left(\frac{-im_r k}{\omega}\right)\sum_{n=1}^{\infty}\sum_{m=-n}^{n} c_n^{pw}\left[c_{mn}\mathbf{M}_{mn}^{(1)} + id_{mn}\mathbf{N}_{mn}^{(1)}\right] \tag{10}$$

For scattered electromagnetic fields, the superscript 3 is employed and the spherical Hankel function of the first kind $h_n^1(kr)$ is included. Furthermore, the spherical Bessel function $j_n(k_1 r)$ is involved in transmitted electromagnetic fields.

The electromagnetic fields satisfy the following boundary conditions (BCs) at the surface of the spherical aerosol particle.

$$\hat{\boldsymbol{r}} \times \left(\boldsymbol{E}^{inc} + \boldsymbol{E}^{sca} - \boldsymbol{E}^{int}\right) = 0 \tag{11}$$

$$\hat{\boldsymbol{r}} \times \left(\boldsymbol{H}^{inc} + \boldsymbol{H}^{sca} - \boldsymbol{H}^{int}\right) = 0 \tag{12}$$

On plucking and substituting the electromagnetic fields of Equations (1) and (2) and Equations (7)–(10) into the above-mentioned BCs, the relationships of the BSCs and expansion coefficients of different electromagnetic fields, including incident, scattered, and internal, can be achieved as

$$a_{mn} = a_n g_{n,TM}^m, b_{mn} = b_n g_{n,TE}^m \tag{13}$$

$$c_{mn} = c_n g_{n,TM}^m, d_{mn} = d_n g_{n,TE}^m \tag{14}$$

where a_n and b_n represent Mie scattering coefficients while c_n and d_n are internal field coefficients.

$$a_n = \frac{[xj_n(x)]'\mu m_r^2 j_n(m_r x) - \mu_1 j_n(x)[m_r x j_n(m_r x)]'}{\left[xh_n^{(1)}(x)\right]'\mu m_r^2 j_n(m_r x) - \mu_1 h_n^{(1)}(x)[m_r x j_n(m_r x)]'} \tag{15}$$

$$b_n = \frac{\mu_1[xj_n(x)]' j_n(m_r x) - \mu[m_r x j_n(m_r x)]' j_n(x)}{j_n(m_r x)\mu_1\left[xh_n^{(1)}(x)\right]' - \mu[m_r x j_n(m_r x)]' h_n^{(1)}(x)} \tag{16}$$

$$c_n = \frac{j_n(x)\mu_1\left[xh_n^{(1)}(x)\right]' - \mu_1[xj_n(x)]'h_n^{(1)}(x)}{j_n(m_r x)\mu_1\left[xh_n^{(1)}(x)\right]' - \mu[m_r x j_n(m_r x)]'h_n^{(1)}(x)} \tag{17}$$

$$d_n = \frac{\mu_1 j_n(x)\left[xh_n^{(1)}(x)\right]' m_r - \mu_1 h_n^{(1)}(x)[xj_n(x)]' m_r}{\mu j_n(m_r x)\left[xh_n^{(1)}(x)\right]' m_r^2 - \mu_1 h_n^{(1)}(x)[m_r x j_n(m_r x)]'} \tag{18}$$

where $x = ka$ indicates the dimensionless size parameter of the spherical aerosol particle. Also, m_r signifies the relative refractive index.

By introducing the Riccati–Bessel functions, the scattering field coefficients can be simplified as

$$a_n = \frac{m_r\psi_n'(x)\psi_n(m_r x) - \psi_n'(m_r x)\psi_n(x)}{m_r\psi_n(m_r x)\xi_n'(x) - \psi_n'(m_r x)\xi_n(x)} \tag{19}$$

$$b_n = \frac{\psi_n'(x)\psi_n(m_r x) - m_r\psi_n'(m_r x)\psi_n(x)}{\psi_n(m_r x)\xi_n'(x) - m_r\psi_n'(m_r x)\xi_n(x)} \tag{20}$$

The optical efficiencies, i.e., extinction efficiency (Q_{ext}), scattering efficiency (Q_{sca}), and absorption efficiency (Q_{abs}), are usual dimensionless parameters in GLMT/Mie-dependent scattering. These quantities are given as the ratio of the corresponding cross-sections to the geometrical cross-section of the spherical particle as $Q_{ext} = \frac{C_{ext}}{\pi a^2}$, $Q_{sca} = \frac{C_{sca}}{\pi a^2}$, $Q_{abs} = \frac{C_{abs}}{\pi a^2}$. where πa^2 denotes the geometrical cross-sectional area while a is the particle radius. The notation C_{ext}, C_{sca}, and C_{abs} characterizes cross-sections of a spherical particle interacting with an electromagnetic wave/beam. Q_{ext} represents the total power detached from the incident wave, while Q_{sca} signifies power redirected by electromagnetic scattering. Q_{abs} denotes power dissipated inside a spherical particle. According to the energy conservation principle, $Q_{ext} = Q_{sca} + Q_{abs}$ holds very well.

By employing the expansion coefficients of scattered fields, the efficiencies (extinction, scattering, and absorption) can be calculated as

$$Q_{ext} = \frac{2}{\rho^2}\sum_{n=1}^{\infty}\sum_{m=-n}^{n}\frac{2n+1}{n(n+1)}\frac{(n+|m|)!}{(n-|m|)!}Re\left(a_n\left|g_{n,TM}^m\right|^2 + b_n\left|g_{n,TE}^m\right|^2\right) \tag{21}$$

$$Q_{sca} = \frac{2}{\rho^2}\sum_{n=1}^{\infty}\sum_{m=-n}^{n}\frac{2n+1}{n(n+1)}\frac{(n+|m|)!}{(n-|m|)!}\left(|a_n|^2\left|g_{n,TM}^m\right|^2 + |b_n|^2\left|g_{n,TE}^m\right|^2\right) \tag{22}$$

$$Q_{abs} = Q_{ext} - Q_{sca} \tag{23}$$

Since aerosol particles are polydispersed, they obey the lognormal distribution model, which is given as

$$N(r) = \frac{dN}{dD} = \frac{1}{\sqrt{2\pi}\ln(\sigma)}\frac{1}{D}\exp\left[-\frac{(\ln(D) - \ln(r_m))^2}{2\,ln^2(\sigma)}\right] \tag{24}$$

Here, D is the diameter, r_m represents the average radius of the scattered particles, and σ be the geometric standard deviation.

Now the average of efficiencies, i.e., extinction, scattering, and absorption, over the lognormal distribution is taken because real atmospheric aerosols scatter light differently and not all of these aerosol particles are the same size.

$$\text{Average efficiency factors} = < Q_{ext,sca,abs} > = \frac{\pi\int_{r_{min}}^{r_{max}} r^2 Q_{ext,sca,abs}(r)\; n(r)dr}{\int_{r_{min}}^{r_{max}} n(r)dr} \tag{25}$$

So, the total beam energy attenuation of GVB at the propagation distance z can be given as

$$\gamma = 4.343\left(\frac{\pi\int_{r_{min}}^{r_{max}} r^2 Q_{ext,sca,abs}(r)\ n(r)dr}{\int_{r_{min}}^{r_{max}} n(r)dr}\right)z \tag{26}$$

This directly connects aerosol particle scattering to communication deterioration. On the basis of the Beer–Lambert law, the atmospheric transmission response of GVBs over a multi-aerosol environment can be expressed as

$$T = e^{-\gamma z} \tag{27}$$

3. Results and Discussion

In this section, all the numerical results are plotted, and the effects on average efficiency factors, including extinction, scattering, and absorption in addition to attenuation and transmission, are discussed. These optical characteristics depend on the configuration parameters of the twisted GVB, including OAM mode index and beam waist radius, and the different aerosol types. In the present work, the aerosol particles are considered spherical scatterers, so fortunately, GLMT works very well. The beam parameters are fixed at λ = 0.55 μm, l = 1, and w_0 = 1.0 mm, unless otherwise mentioned. For different aerosol particles, the refractive indices are adopted, which are mentioned in Table 1.

Table 1. The refractive index of different aerosol particles when the operating wavelength of the vortex light beam is at λ = 0.55 μm.

Aerosol Types	Real Part	Imaginary Part
Unformed Carbon	1.98	0.232
Dust	1.52	0.0034
Silicate	1.7175	0.0294
Sulphate	1.52	10^{-7}
Nitrate	1.55	10^{-8}
Soot	1.80	0.54

This study is based on an operating wavelength of 0.55 μm for the analysis of GVB scattering in an aerosol-mediated atmosphere. This wavelength falls in the visible optical domain and is generally used in studies of free-space propagation, air scattering and atmospheric scattering. Though current optical communication schemes commonly operate in the near-infrared region, the present work highlights the basic scattering dynamics and phase-distortion response of GVBs under diverse aerosol environments (unformed carbon, dust, sulphate, silicate, soot, and nitrate), where the impact of beam operating wavelength is kept fixed to isolate the effect of aerosol particle refractive index variations.

Scattering impacts of aerosol particles with different size parameters result in different magnitudes of energy loss of GVBs on propagation in different aerosol atmospheres. Efficiency factors $(Q_{ext}, Q_{sca}, Q_{abs})$ can present the usual influences of dimensionless particle size variation and OAM mode index, considering the scattering response of spherical aerosols on GVBs. Therefore, Figure 2 shows the influence of the OAM mode index (l) of GVB on efficiency factors such as $l = 1,\ 2,\ 3$, and 4, respectively. The numerical results indicate that as the OAM mode number increases, it results in a decrease in the efficiency factors. The reason behind this effect is that the internal field modes involve various OAM mode numbers and play a part in the scattering phenomenon. The interaction of GVB with aerosol particles changes the beam profile. A unique electromagnetic scattering

pattern develops with an increase in the OAM mode number. As the OAM mode index increases, there is more twist in the phase profile, and this leads to the scattered intensity distributions. The scattering features of the GVB field with aerosol particles are similar; though, the amplitudes differ slightly in magnitude, and they decrease as the OAM mode number increases.

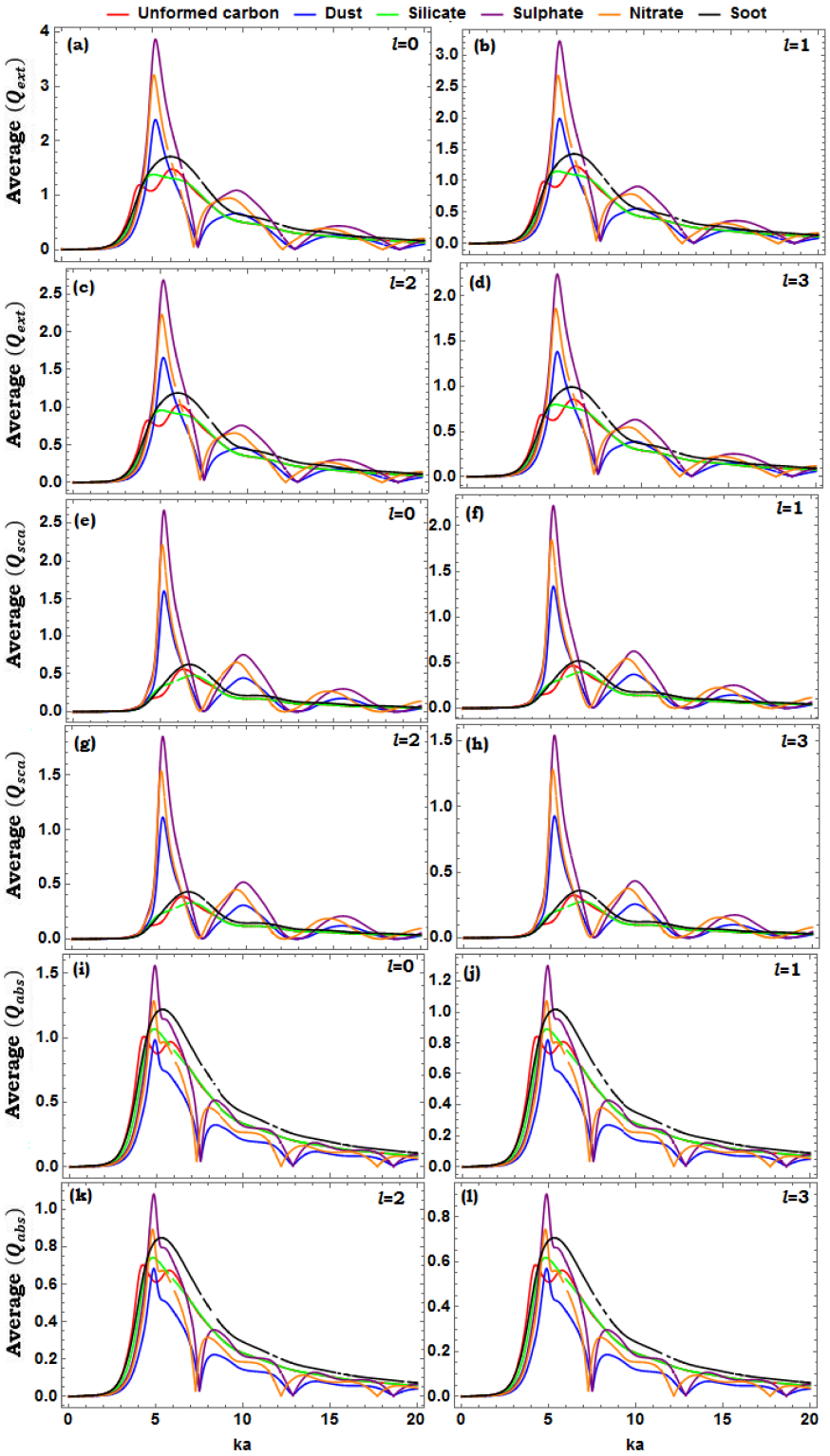


Figure 2. The average extinction, scattering, and absorption efficiency of various aerosols when interacting with GVBs with different OAM mode numbers (**a**–**d**) average Q_{ext} (**e**–**h**) average Q_{sca} (**i**–**l**) average Q_{abs}. The OAM mode numbers are mentioned in each of the panels.

The efficiencies firstly increase with the dimensionless size parameter of aerosol particles and then decrease after a peak value; thereafter, their behavior becomes gradually stable. The scattering response of structured GVB fields by aerosol scatterers is influenced by the intensity distributions and phase profiles. GVBs have unique intensity distributions, which result in the much-reduced scattering influences of aerosol scatterers compared to those of plane waves and conventional Gaussian beams. For $l = 0$, GVBs transform into non-vortex GBs. Results indicate that the efficiencies for Gaussian beams with a higher-order OAM mode index become smaller compared to those of non-vortex GBs. Furthermore, the intensity distribution and the size of the hollow inner ring of GVBs gradually increase as the OAM mode index increases, yielding a significant difference in their efficiency factors. Higher extinction indicates more loss in communication quality.

It is clearly shown that the efficiencies of different aerosol particles under GVB's incidence are distinctly different; the reason behind that is because of the different refractive indices of aerosol particles. Based on the published literature [15,39], Table 1 indicates the refractive index for incident beam operating wavelengths of 0.55 μm. Its physical significance lies in the fact that the real part characterizes scattering response, while the imaginary part signifies absorption response. The real part also contributes towards Mie resonances.

The realistic environments embrace polluted and marine aerosol particles; hence, absorption and scattering characteristics due to aerosols, air molecules, and water vapors lead to gradual attenuation of the incident beam profile during propagation, generating deterioration of the total efficiency. Also, considering complex environment networks, the understanding of refractive index-based optical responses of GVBs is quite indispensable for evaluating their performance. The refractive index strongly affects both the amplitude and the scattering characteristics. As the refractive index corresponding to each type of aerosol particle differs, the optical energy possessed by the incident GVB also changes, resulting in a change in the effective scattering response. The real and imaginary components of refractive index also modify the balance between scattering and absorption features, and the resulting change tunes the profile of GVBs.

Increasing the OAM mode number results in decreasing the extinction efficiency characteristics; the phenomenon behind this response is the redistribution of the optical energy in higher-order GVBs. Augmenting the OAM mode number from unit value onward, the beam carries an extended annular intensity and a larger phase singularity, yielding an enhanced radial spread and reduced on-axis intensity along the optical axis. So, a smaller part of the incident field energy overlaps with the cross-section of the various aerosol scatterers. This condensed spatial response overlap dictates a weaker interaction of GVB with aerosol particles and consequently results in a lower extinction efficiency.

Moreover, the annular intensity distribution features of GVBs significantly tune their scattering dynamics compared to basic Gaussian beams (GBs). Different from conventional GBs, whose maximum intensity is focused on the propagation optical axis, GVBs display a ring-oriented intensity distribution, causing the beam interaction with spherical aerosols to happen via off-axis scattered electromagnetic fields. These yields varied excitation of scattering modes and reduced forward field coupling, which overall reduces the total extinction efficiency and tunes the scattering response.

In Figure 2, the observed segmented trend shows a numerical artifact instead of a physical phenomenon. This numerical artifact arises from the quick oscillatory nature of Mie resonances, where the optical efficiencies—namely, extinction, scattering, and absorption—vary rapidly with the dimensionless size parameter. These variations form continuous curves. Consequently, all evaluated optical efficiencies remain intrinsically

continuous functions of the size or scale parameter, and no model inconsistency or physical discontinuity is involved in the simulation.

Figure 3 shows that an augmentation in the beam waist radius results in wider beam widths, and the hollow inner ring increases, considering the GVB intensity structure, so the scattered field pattern begins to increase. Increasing the beam's waist, a large amount of incident beam energy is accessible to irradiate the spherical surfaces of the aerosol scatterer, so this energy is distributed during the scattering of GVB. Considering the beam waist radius for a total of efficiency factors, the OAM mode index is fixed as $l = 1$, whereas the beam waist is varied as $w_0 = (0.3, 0.5, 0.7, 0.9)$ mm. Compared to that of a conventional Gaussian beam, the scattered field pattern under the influence of the GVB field does not continually augment with the increase in the waist radius (w_0). The strength of the scattered field distribution depends on the suitable selection of the beam configuration parameters, including OAM mode index and waist radius, in addition to the scale parameter of the aerosol scatterer. Since GVBs with a larger beam width possess more energy to irradiate the scatterer particles, this energy is distributed and augments the total efficiency.

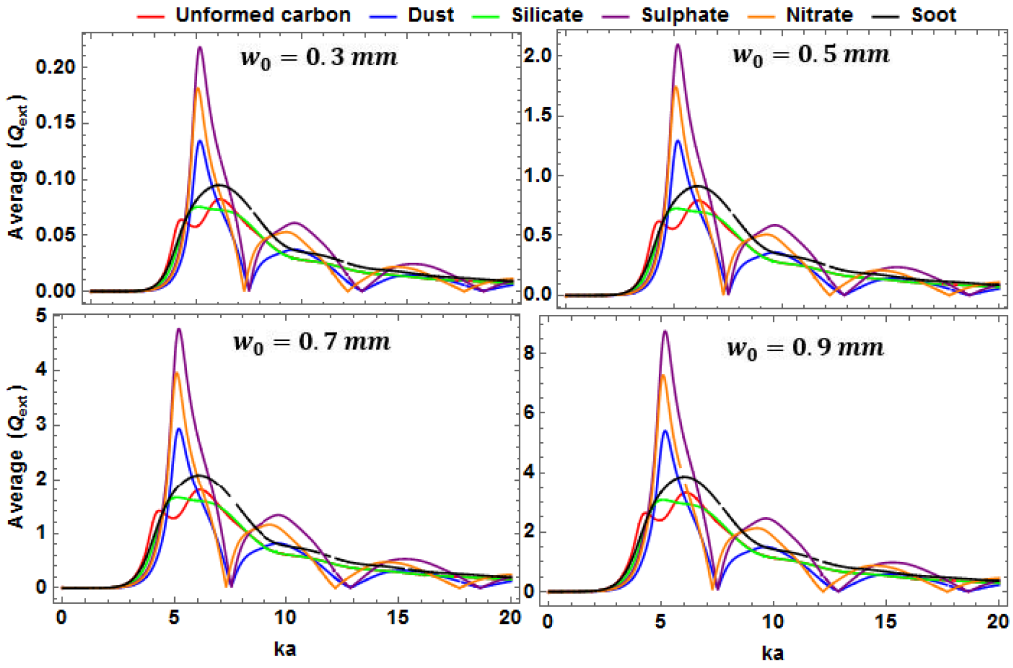


Figure 3. The average extinction efficiency of various aerosol particles irradiated by GVBs with a unit OAM mode index and different beam waist radii, i.e., $w_0 = 0.3$ mm, $w_0 = 0.5$ mm, $w_0 = 0.7$ mm, and $w_0 = 0.9$ mm.

Figure 4 displays the particle distribution for different types of aerosol particles. Implementing the lognormal distribution makes the aerosol particle model more realistic and better depicts particle populations. Different aerosol particles have different configuration parameters, including mean particle radius and spread. Their population responses differ in the context of peak positions and widths of curves. Narrow curves show uniform particle sizes, while wider curves characterize broad size variation. Furthermore, implementing the lognormal distribution results in an average scattering over a range of spherical scatterer sizes, smoothing out the sharp GLMT resonance scattering peaks in terms of realistic continuous curves.

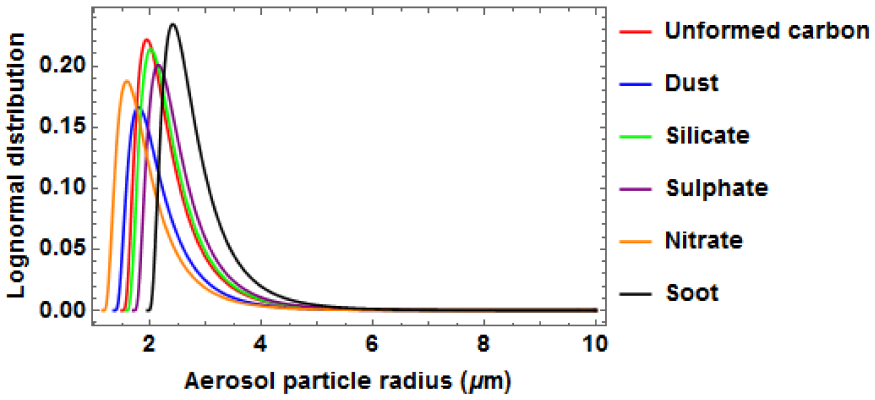


Figure 4. Distribution for different aerosol particles versus radius (μm).

Figure 5 displays the attenuation rate for varying OAM mode numbers of GVB for diverse aerosol particles. The attenuation response of GVBs significantly changes with variations and increases in propagation distance. The results indicate that GVBs carrying OAM can advance attenuation features while still conserving most of the transmitted information, yielding lower signal or data loss during propagation through different aerosol particles. The curves for various OAM values have similar attenuation tendencies, and the attenuation rate of GVB transmission in the different aerosol atmospheres increases with an increase in propagation distance. Increasing the OAM mode number leads to a broader intensity distribution and a more significant phase profile of the beam, augmenting the interaction of vortex beams with aerosol scatterers and usually increasing extinction and scattering losses. A greater increase in attenuation with higher-order GVB is found for highly absorbing aerosol particles, including soot, with little increase exposed for weakly absorbing aerosol particles like nitrate. Higher attenuation results in deteriorated multimedia transmission. Consequently, higher-order vortex beams are more attenuated, but these can deliver robust information transfer because of the degree of freedom of the OAM for communication channels.

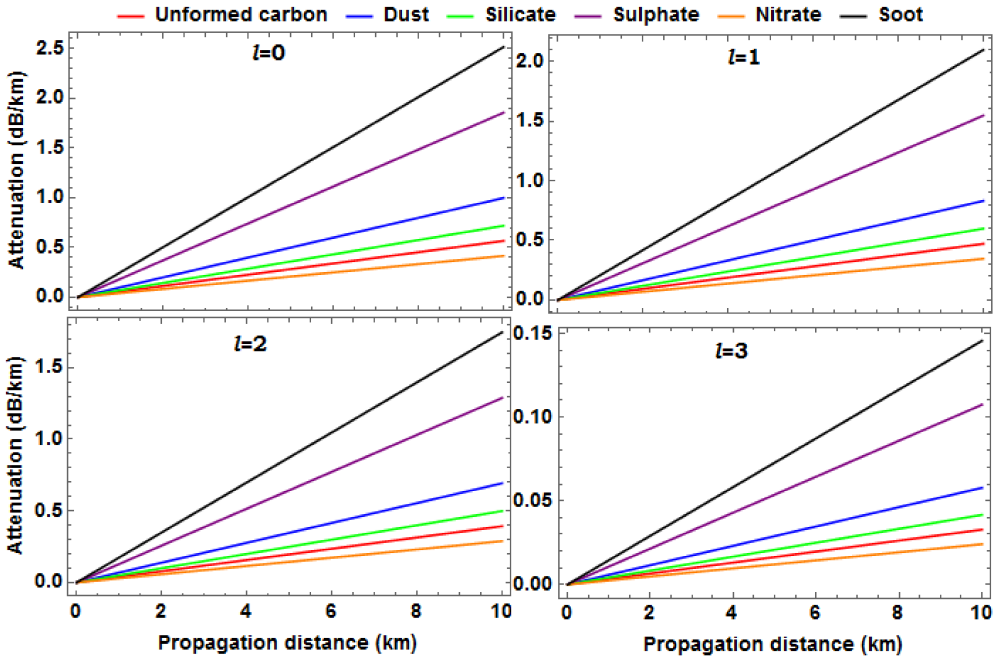


Figure 5. Attenuation rate of GVB for different aerosol particles under different OAM mode numbers, i.e., $l = 0,\ 1,\ 2$, and 3, versus propagation distance.

In Figure 6, we analyze the transmissivity of GVBs with different OAM mode numbers and varying link distances through diverse aerosol atmospheric transmission. The OAM mode index influences the transmission response of a GVB by tuning the energy distribution and beam shape. The higher-order GVBs generate a larger annular intensity distribution, which could enhance the modal information capacity and spatial robustness through various aerosol propagations. The OAM mode index directly influences the transmission stability and resilience of the vortex beam in aerosol communication channels. GVB with a higher OAM mode index has a stronger penetration ability in an aerosol environment because of the weaker extinction efficiency caused by aerosol scatterers. The transmission rate of GVB in an aerosol environment decreases with the increase in propagation distance. A small value of transmissivity represents weak attenuation and a weaker received signal, while large values designate intense channel fading. Table 2 shows the quality characteristics against the transmissivity of GVBs through atmospheric aerosol particles.

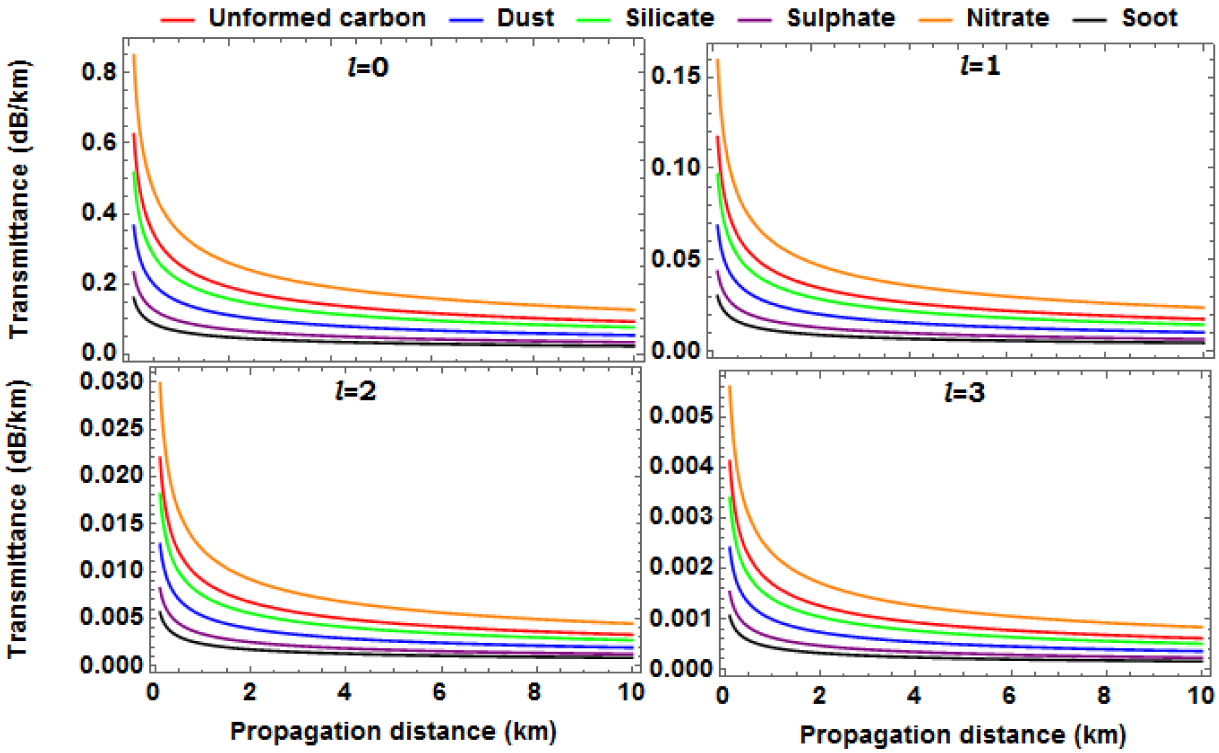


Figure 6. Transmission rate of GVB for different aerosol particles under different OAM mode numbers, i.e., $l = 0, 1, 2, 3$, versus propagation distance.

Table 2. Transmissivity of GVBs via atmospheric-induced aerosol with channel fading.

Transmissivity (T)	Channel Response
T << 1.0	Failure of communication
T < 0.5	High deterioration
T ≈ 1.0	Excellent performance

For soot aerosols, absorption is very high, while multimedia transmission ability is very poor. Furthermore, the attenuation response is very weak. For nitrate aerosols, mainly scattering dominates, while it also results in weak absorption. It contributes to better communication. Considering dust aerosol particles, severe beam distortion and high particle scattering are involved. Silicate aerosols show a moderate optical response.

To verify the present theory and coding, the scattering efficiency of some aerosol particles is computed. Some of the polluted aerosol particles in the hazy atmosphere, such as carbonaceous aerosol, ammonium nitrate aerosol, and marine aerosol, are considered. Based on Hanel's humidity equivalent model, a comparison is made for some limiting conditions. Under the operating wavelength of GVB, i.e., λ = 0.55 μm, the complex refractive indices of the aforementioned aerosol particles are $1.750 - 0.44i$, $1.554 - 10^{-8}i$, and $1.333 - 1.96 \times 10^{-8}i$, respectively. For OAM mode index $l = 0$, the GVB reduces to a non-vortex basic Gaussian beam. The results ensure the fair conformity of scattering of plane waves and conventional Gaussian beams by some of the spherical aerosol particles. This validation of numerical results can be observed in Figure 7.

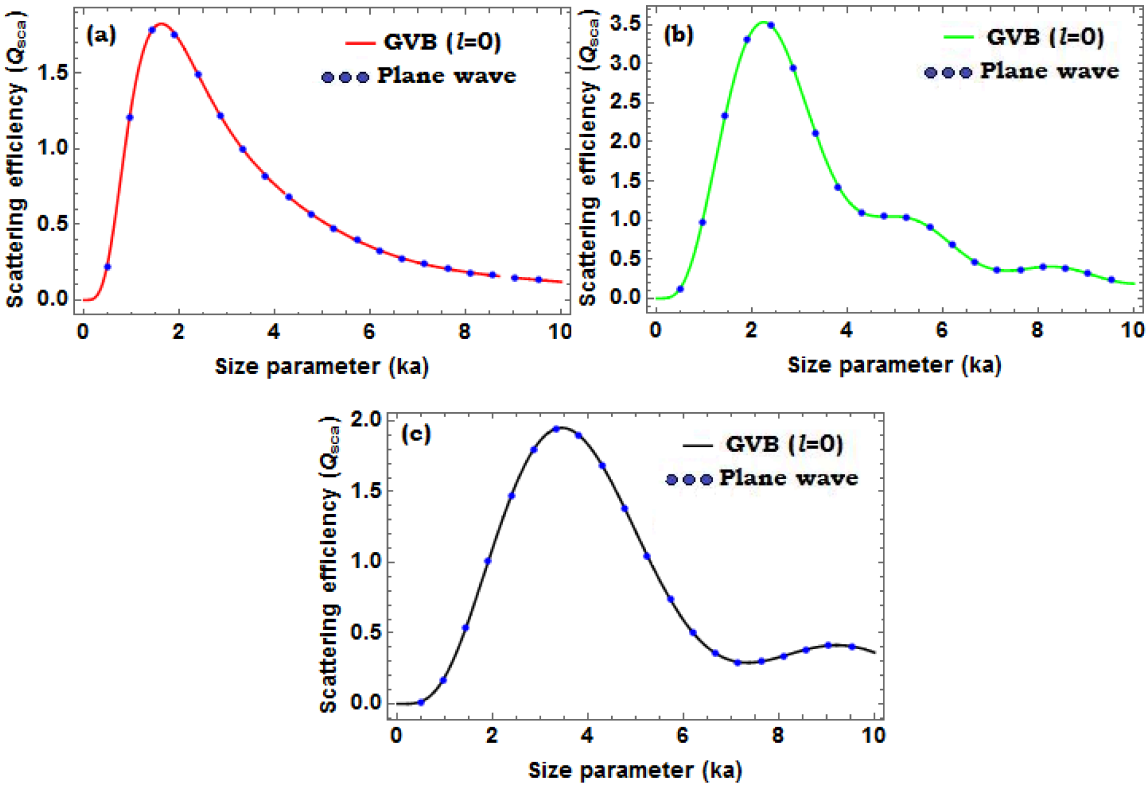


Figure 7. Comparison of scattering efficiency for a special condition, i.e., GVB for $l = 0$ and plane wave for various aerosol particles, (**a**) carbonaceous aerosol, (**b**) ammonium nitrate aerosol, and (**c**) marine water aerosol. For non-vortex GVB ($l = 0$), the results of the present formulation transform into plane wave scattering by corresponding spherical aerosol particles.

Figure 7 consists of three panels, i.e., a, b, and c. The scattering efficiency is plotted for all the aforementioned panels for the OAM mode index $l = 1$ and plane waves. For Figure 7a–c, the target aerosol particles are used as carbonaceous aerosol, ammonium nitrate aerosol, and marine water aerosol, respectively.

The comparison of the present results is made with our prior research on (i) scattering dynamics of marine aerosol particles under illumination of a Laguerre–Gaussian (LG) beam and (ii) Bessel vortex beam (BVB) scattering by a perfect electromagnetic conductor (PEMC) sphere. Though a direct measurable quantitative comparison is not reasonable because of differences in beam configuration parameters, scatterer models, and beam structures, a meaningful qualitative comparison can be framed between different scattering systems.

For all the aforementioned studies, the scattering response is tuned by the nature of the scatterer and the vortex beam's spatial structure. Nevertheless, the present analysis displays unique features because of the interaction of the Gaussian vortex beam (GVB)

with realistic polluted atmospheric spherical aerosols, where both propagation impacts and aerosol-mediated attenuation, besides transmission response, play a substantial role. This is different from the LG-beam case, which remains limited to a single marine aerosol particle, and the BVB case, which considered an idealized PEMC spherical scatterer.

A comparison table can be viewed as Table 3, which summarizes these variations and highlights the uniqueness of the present work.

Table 3. Comparison of the present work and previously analyzed different vortex beam scattering studies.

Studies	Vortex Beams	Spherical Scatterer	Physical Modeling	Focusing	Findings
Previously published work Ref. [18]	LG vortex beam	Single marine aerosol particle	Marine atmosphere	Differential scattering cross-section (DSCS) and aerosol dependence	Strong scattering sensitivity to refractive index, aerosol size, radial, and azimuthal mode dependence
Previously published work Ref. [11]	BVB	PEMC sphere	Idealized PEMC boundary	Scattering/radar cross-section (RCS) behavior	Topologically mediated and electromagnetic scalar admittance-based optical efficiencies
Present work	GVB	Various types of atmospheric aerosol particles	Realistic propagation over different aerosol media	Scattering, transmission, and attenuation over propagation distance	Overall impact of various aerosol particles and propagation distance on beam quality

The original electric field of the GVB can be characterized at the source plane as

$$\boldsymbol{E}^{ori}(r,\varphi,0) = E_0\left(\frac{r}{w_0}\right)^l \exp\left[\frac{-r^2}{w_0^2}\right]\exp(il\varphi) \tag{28}$$

Figure 8 shows the transverse electric field intensities. Figure 8a shows the original electric field characterized as E^{ori} and defined by Equation (28), whereas Figure 8b represents the reconstructed field indicated as E^{rec} using BSCs of GVB and given in Equation (1). The relative error (ϵ) is expressed as $\epsilon = \frac{|E^{ori}-E^{rec}|}{|E^{ori}|}$, and is also plotted in Figure 8c. The error occurs because of numerical integration during the ILA method and terms such as $ik\sqrt{(r^2+z^2)}$ oscillate quickly for large wave numbers. Nonetheless, the inconsistencies are still insignificant. As we have employed x-linearly polarized GVB, the numerical error will vary with various states of polarization and OAM mode index l.

To demonstrate the influence of aerosol scattering on the phase profile of the GVB, the phase distributions before and after interaction are given in Figure 9. The resulting phase distortion has wavefront degradation.

The interaction of the GVB with various aerosol particles can add phase distortion because of optical characteristics, including scattering and absorption. This results in a variation in the original helical phase profile of the beam. However, this distortion is based on the size parameter, particle refractive index, and configuration parameters of GVB. The present study deals with the impact of different aerosol scatterers through their scattering dynamics, which designates the degree of perturbation added into the propagating GVB. A higher scattering response indicates a stronger possibility of phase degradation of OAM mode orthogonality, which can increase crosstalk channels in communication systems. For practical communication systems, the distorted GVB can still be employed by applying appropriate signal processing techniques, including phase compensation, adaptive wave-

front correction, or mode reconstruction corresponding to the receiver plane. The present study deals with the scattering-induced understanding required for assessing such impacts, whereas a detailed investigation of OAM channel capacity and phase recovery will be explored in future studies.

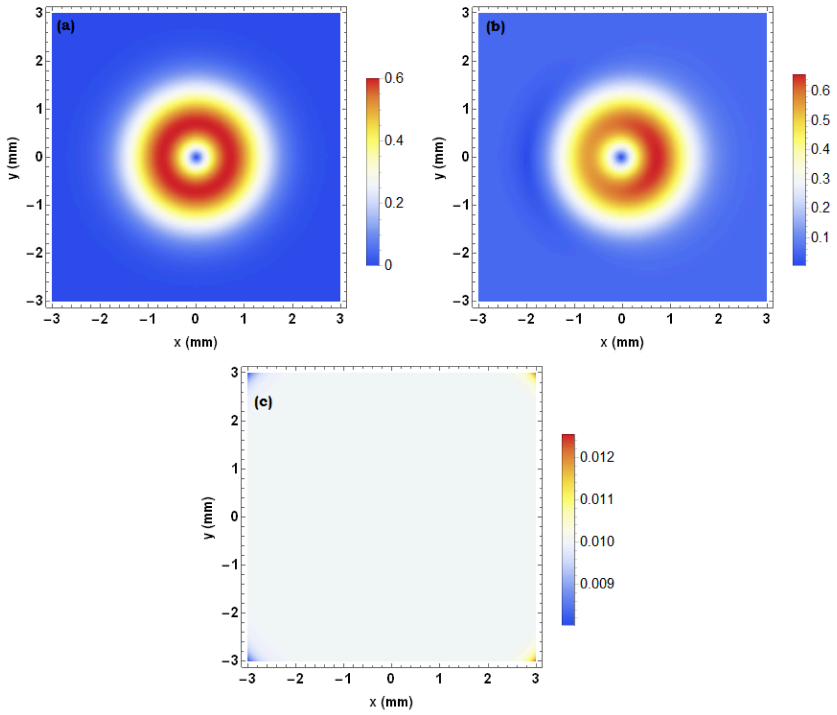


Figure 8. Spatial distributions of the electric fields for an x-linearly polarized GVB with $\lambda = 0.55$ μm, $l = 1$, and $w_0 = 1.0$ mm, (**a**) the original electric field given by Equation (28), (**b**) the reconstructed electric field from Equation (1), and (**c**) the calculated relative error.

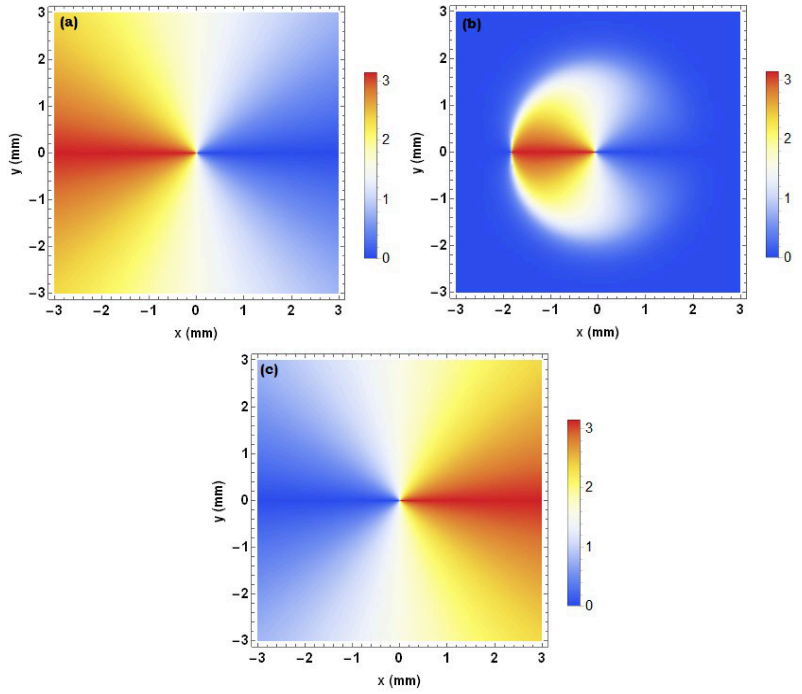


Figure 9. Phase distribution of GVB (**a**) incident field, (**b**) scattered field after interaction with aerosol particles, and (**c**) corresponding phase difference in wavefront distortion.

The backward-scattering efficiency (Q_b) is given as

$$Q_b = \frac{1}{\rho^2}\left|\sum_{n=1}^{\infty}\sum_{m=-n}^{n}\frac{2n+1}{n(n+1)}\frac{(n+|m|)!}{(n-|m|)!}(-1)^n\left(a_n g_{n,TM}^m - b_n g_{n,TE}^m\right)\right|^2 \quad (29)$$

The backward-scattering efficiency (backscattering factor) for different spherical aerosol particles, such as unformed carbon, dust, sulphate, silicate, soot, and nitrate, at an operating wavelength of 0.55 μm and OAM mode index $(l = 1)$ is analyzed in Figure 10. The backward-scattering efficiency shows a strong dependence on the types of aerosol particles. Sulphate and nitrate aerosol particles show the maximum backward efficiency because of their strong elastic scattering response and weak absorption. Silicate and dust particles exhibit intermediate values due to their moderate absorption characteristics and mixed values of refractive index. Compared to the aforementioned aerosol particles, unformed carbon and soot aerosols display the lowest backward efficiency due to higher absorption losses, which substantially reduces the backscattered field distribution. This response is characterized by the collective impact of optical characteristics, i.e., scattering, absorption and refractive index contrast, which tunes the amplitude and phase of the GVB-based scattering field coefficients, thus influencing the interference phenomena in the backward direction. The presence of this result will also assist in enhancing the relevance of the present work for lidar-based optical sensing and communication applications.

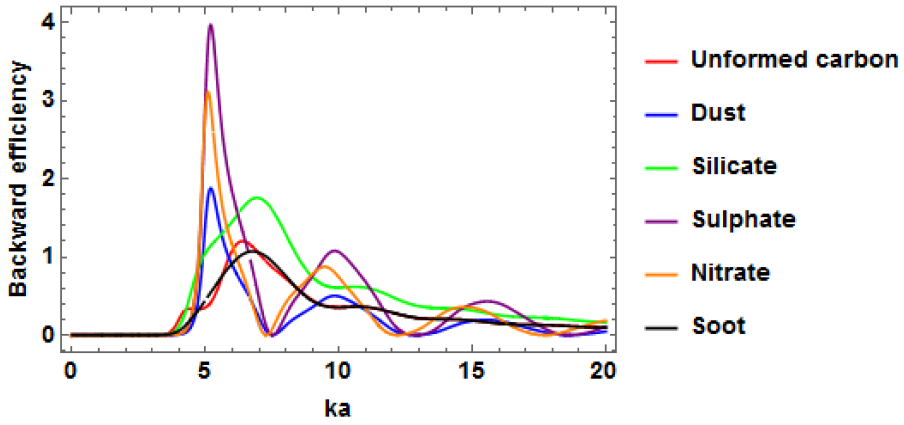


Figure 10. Backward-scattering efficiency of GVB for different aerosol particles (unformed carbon, dust, sulphate, silicate, soot, and nitrate) at $l = 1$, w_0 = 1.0 mm, and λ = 0.55 μm.

Nevertheless, a quantitative analysis of angular momentum transfer between the GVB and spherical aerosol particles, including calculation of optical torque and related mechanical impacts, is out of the scope of the existing GLMT-based theoretical scattering model. In the proposed work, the focus remains on the electromagnetic scattering dynamics of the vortex beam, while the mechanical consequences of OAM exchange are not explicitly assessed.

These results suggest that GVBs have many advantages for OAM-based scattering studies. Since OAM-based studies are essential for understanding scattering, propagation, and transmission, the combination of attenuation, transmission, and efficiency factors may support the exploration of various atmospheric characteristics. The observed sensitivity and scattering pattern in relation to beam configuration parameters provide theoretical insights into active aerosol lidar (light detection and ranging) schemes that require control over structured light beams. For atmospheric aerosols, this characteristic is very significant, as it connects the extinction features of atmospheric aerosols. Furthermore, an OAM-based environment provides resilience over vortex characteristics, so the OAM-induced scattering

peaks and lobes permit OAM filtering and sorting. This feature is quite advantageous in communication systems and sensing networks.

The conceivable implications of the research include reliability of enhanced OAM-based radar cross-section (OAM-RCS), enhanced optical manipulation of structured light beams, OAM-based optical characteristics, optimizing configuration beam parameters of GVBs for nonlinear optics, and potential for improved free-space optical (FSO) communication. It also includes enhanced modeling of the propagation of structured light beams through marine and polluted atmospheres. Optimizing configuration beam parameters for rigorous atmospheric transmission may result in enhanced remote sensing of diverse aerosol particles.

4. Conclusions

The continuous interaction of electromagnetic waves and structured light beams propagating in the free-space atmosphere with suspended aerosol-rich particles has a substantial impact on image contrast, signal propagation, and transmission quality, resulting in significant deviations from the original information. So, the scattering characteristics of aerosol particles were analyzed extensively by employing the lognormal distribution model for the atmospheric channel. Following the analytical formulation and numerical analysis, this study further discusses the impact of configuration beam parameters and aerosol-laden environments on optical characteristics, including scattering, attenuation, and transmission. Numerical results indicate that the penetration ability of a high-order GVB in an aerosol-laden environment is much stronger compared to a conventional Gaussian beam ($l = 0$). To characterize the optical characteristics of GVBs, the complex refractive index of aerosol particles plays a significant role. The complex refractive index of a given aerosol particle varies with the incident operating wavelength, which results in tuning the scattering response. Scattering through aerosol particles causes spreading of the OAM spectrum, information degradation, mode distortion, and distortion in the OAM phase profile. With the increase in propagation distance and OAM mode number, the energy attenuation of GVB decreases, considering the diverse aerosol environment. The scintillation index (SI), which symbolizes intensity distortions under atmospheric turbulence, is not calculated in the present study because of the deterministic nature of the GLMT-dependent different spherical aerosol scattering model. This analysis is left for future works, including random atmospheric variations. The application of GVBs through atmospheric spherical aerosols furnishes a satisfactory platform for cutting-edge environmental remote sensing and sensing applications, offering a fine paradigm for FSO communication systems that embrace rigorous and dynamic signal strength. The efficiency of multimedia information transmission can be improved by implementing the scattering algorithm to invert the distribution and configuration of aerosol particles. These findings also signify the scattering response of GVBs in aerosol-laden surroundings and highlight their potential for robust optical communication over maritime channels and OAM-mediated environmental monitoring.

Author Contributions: Conceptualization, methodology, software, validation, writing—review and editing, and writing—original draft preparation, B.A., F.R., M.A.; supervision, M.A.; project administration, B.A., F.R.; funding acquisition, B.A., F.R. All authors have read and agreed to the published version of the manuscript.

Funding: Prince Sattam bin Abdulaziz University for funding with the project number (PSAU/2025/01/37271).

Institutional Review Board Statement: Not applicable.

Informed Consent Statement: Not applicable.

Data Availability Statement: All data that support the findings of the study have been included in the manuscript.

Acknowledgments: The authors extend their appreciation to Prince Sattam bin Abdulaziz University for funding this research work through the project number (PSAU/2025/01/37271).

Conflicts of Interest: The authors declare no conflicts of interest.

Abbreviations

The following abbreviations are used in this manuscript:

OAM	Orbital angular momentum
GVBs	Gaussian vortex beams
GLMT	Generalized Lorenz–Mie theory
BSCs	Beam shape coefficients
VSWFs	Vector spherical wave functions
BCs	Boundary conditions
FSO	Free-space optical

References

1. Allen, L.; Beijersbergen, M.W.; Spreeuw, R.; Woerdman, J. Orbital angular momentum of light and the transformation of Laguerre-Gaussian laser modes. *Phys. Rev. A* **1992**, *45*, 8185–8189. [CrossRef] [PubMed]
2. Padgett, M.; Courtial, J.; Allen, L. Light's orbital angular momentum. *Phys. Today* **2004**, *57*, 35–40. [CrossRef]
3. Padgett, M. Light's twist. *Proc. R. Soc. A Math. Phys. Eng. Sci.* **2014**, *470*, 20140633.
4. Cheng, M.; Jiang, W.; Guo, L.; Li, J.; Forbes, A. Metrology with a twist: Probing and sensing with vortex light. *Light Sci. Appl.* **2025**, *14*, 4. [CrossRef] [PubMed]
5. Kotlyar, V.V.; Kovalev, A.A.; Porfirev, A.P. *Vortex Laser Beams*; CRC Press: Boca Raton, FL, USA, 2018.
6. Kovalev, A.A.; Kotlyar, V.V.; Porfirev, A.P. Orbital angular momentum and topological charge of a multi-vortex Gaussian beam. *J. Opt. Soc. Am. A* **2020**, *37*, 1740–1747. [CrossRef] [PubMed]
7. Long, L.; Hao, X.; Qiang, F. Research progresses in theory and applications of vortex electromagnetic waves. *J. Microw.* **2018**, *34*, 1–12.
8. Zhou, G.-Q. Far Field Structural Properties of a Gaussian Vortex Beam. *Lasers Eng.* **2013**, *26*, 1–17.
9. Wang, Y.; Guo, M.; Wu, J.; Liu, J.; Yang, X.; Li, J. Propagation of Gaussian vortex beams in electromagnetically induced transparency media. *Opt. Express* **2022**, *30*, 43426–43438. [CrossRef] [PubMed]
10. Forbes, A.; De Oliveira, M.; Dennis, M.R. Structured light. *Nat. Photonics* **2021**, *15*, 253–262. [CrossRef]
11. Arfan, M.; Asif, M.; Ghaffar, A.; Razzaz, F.; Saeed, S.; Alanazi, T. Analysis of Scattering characteristics of PEMC sphere by vortex Bessel beams. *Optik* **2024**, *298*, 171599.
12. Khanom, F.; Mohamed, N.; Lopushenko, I.; Sdobnov, A.; Doronin, A.; Bykov, A.; Rafailov, E.; Meglinski, I. Twists through turbidity: Propagation of light carrying orbital angular momentum through a complex scattering medium. *Sci. Rep.* **2024**, *14*, 20662. [CrossRef] [PubMed]
13. Meglinski, I.; Lopushenko, I.; Sdobnov, A.; Bykov, A. Phase preservation of orbital angular momentum of light in multiple scattering environment. *Light Sci. Appl.* **2024**, *13*, 214. [CrossRef] [PubMed]
14. Huang, Q.; Cheng, M.; Guo, L.; Li, J.; Yan, X.; Liu, S. Scattering of aerosol particles by a Hermite–Gaussian beam in marine atmosphere. *Appl. Opt.* **2017**, *56*, 5329–5335. [CrossRef] [PubMed]
15. Qu, T.; Li, H.; Wu, Z.; Shang, Q.; Wu, J.; Kong, W. Scattering of aerosol by a high-order Bessel vortex beam for multimedia information transmission in atmosphere. *Multimed. Tools Appl.* **2020**, *79*, 34159–34171. [CrossRef]
16. Shi, C.; Guo, L.; Cheng, M.; Li, R. Scattering of a high-order vector Bessel Gaussian beam by a spherical marine aerosol. *J. Quant. Spectrosc. Radiat. Transf.* **2021**, *265*, 107552. [CrossRef]
17. Li, J.; Carlson, B.E.; Yung, Y.L.; Lv, D.; Hansen, J.; Penner, J.E.; Liao, H.; Ramaswamy, V.; Kahn, R.A.; Zhang, P. Scattering and absorbing aerosols in the climate system. *Nat. Rev. Earth Environ.* **2022**, *3*, 363–379. [CrossRef]
18. Arfan, M.; Ghaffar, A.; Alkanhal, M.A.; Khan, Y.; Alqahtani, A.; Shakir, I. Laguerre–Gaussian beam scattering by a marine aerosol. *Opt. Quant. Electron.* **2023**, *55*, 756. [CrossRef]
19. Miles, R.E.; Carruthers, A.E.; Reid, J.P. Novel optical techniques for measurements of light extinction, scattering and absorption by single aerosol particles. *Laser Photonics Rev.* **2011**, *5*, 534–552. [CrossRef]

20. Moosmüller, H.; Chakrabarty, R.; Arnott, W. Aerosol light absorption and its measurement: A review. *J. Quant. Spectrosc. Radiat. Transf.* **2009**, *110*, 844–878. [CrossRef]
21. Arfan, M.; Asif, M.; Alkhoori, H.M. Orbital angular momentum based scattering characteristics for foggy atmosphere. *Opt. Quant. Electron.* **2024**, *56*, 630. [CrossRef]
22. Zhang, H.; Zhu, J.a.; Lu, X.; Hu, Z.; Gao, J.; Liu, K.; Zhan, Q.; Cai, Y.; Zhao, C. Single-shot phase retrieval for randomly fluctuated and obstructed vortex beams. *Sci. China Phys. Mech. Astron.* **2024**, *67*, 244211. [CrossRef]
23. Cui, Z.; Jin, Q.; Ding, J.; Ren, X.; Zhang, H.; Tang, Z.; Yang, X.; Zhang, H.; Liu, K.; Li, X. Recognition of fractional topological charge through self-rotating beam phase. *Appl. Phys. Lett.* **2025**, *127*..
24. Zhang, H.; Li, X.; Ma, H.; Tang, M.; Li, H.; Tang, J.; Cai, Y. Grafted optical vortex with controllable orbital angular momentum distribution. *Opt. Express* **2019**, *27*, 22930–22938. [CrossRef] [PubMed]
25. Zhang, H.; Zeng, J.; Lu, X.; Wang, Z.; Zhao, C.; Cai, Y. Review on fractional vortex beam. *Nanophotonics* **2022**, *11*, 241–273. [PubMed]
26. Hänel, G. The properties of atmospheric aerosol particles as functions of the relative humidity at thermodynamic equilibrium with the surrounding moist air. In *Advances in Geophysics*; Elsevier: Amsterdam, The Netherlands, 1976; pp. 73–188.
27. Hänel, G. New results about the sizes of atmospheric aerosol particles as functions of the relative humidity. *Appl. Opt.* **1998**, *27*, 2287–2295.
28. Fraser, R.S.; Kaufman, Y.J. The relative importance of aerosol scattering and absorption in remote sensing. *IEEE Trans. Geosci. Remote Sens.* **1985**, *GE-23*, 625–633. [CrossRef]
29. Schmale, J.; Zieger, P.; Ekman, A.M. Aerosols in current and future Arctic climate. *Nat. Clim. Change* **2021**, *11*, 95–105. [CrossRef]
30. Shi, C.; Guo, L.; Cheng, M.; Lavery, M.P.; Liu, S. Aerosol scattering of vortex beams transmission in hazy atmosphere. *Opt. Express* **2020**, *28*, 28072–28084. [CrossRef] [PubMed]
31. Porfirev, A.P.; Kirilenko, M.S.; Khonina, S.N.; Skidanov, R.V.; Soifer, V.A. Study of propagation of vortex beams in aerosol optical medium. *Appl. Opt.* **2017**, *56*, E8–E15. [CrossRef] [PubMed]
32. Song, H.; Zhang, R.; Hu, N.; Zhou, H.; Su, X.; Song, H.; Zou, K.; Pang, K.; Liu, C.; Park, D. Dynamic aerosol and dynamic air-water interface curvature effects on a 2-Gbit/s free-space optical link using orbital-angular-momentum multiplexing. *Nanophotonics* **2022**, *11*, 885–895. [PubMed]
33. Hou, J.; Sun, X.; He, C.; Wan, X.; Wang, W.; Tian, Z.; Zhou, S.; Liu, W.; Cheng, J.; Wang, S. Transmission characteristics of Laguerre–Gaussian vortex beams under scattering in a smoky environment. *Opt. Commun.* **2026**, *606*, 132876. [CrossRef]
34. Yan, B.; McGloin, D. Three-Dimensional Trapping Dynamics of Aerosols Using Laguerre-Gaussian Vortex Beams. In *Proceedings of the 2024 IEEE Photonics Conference (IPC)*; IEEE: New York, NY, USA, 2024.
35. Yali, R.; Yufeng, W.; Zeping, S.; Qing, G.; Huige, D.; Yuehui, S.; Dengxin, H. Investigation of a vortex beam-based inversion method for aerosol particle size distribution. *Opt. Express* **2024**, *32*, 47515–47531. [CrossRef]
36. Gouesbet, G.; Gréhan, G. *Generalized Lorenz-Mie Theories*; Springer: Berlin/Heidelberg, Germany, 2011; Volume 31.
37. Gouesbet, G.; Gréhan, G.; Maheu, B.; Ren, K.F. *Electromagnetic Scattering of Shaped Beams (Generalized Lorenz–Mie Theory)*; LESP, CORIA, INSA de Rouen: Saint Etienne du Rouvray, France, 1998.
38. Ren, K.F.; Gouesbet, G.; Gréhan, G. Integral localized approximation in generalized Lorenz–Mie theory. *Appl. Opt.* **1998**, *37*, 4218–4225. [CrossRef] [PubMed]
39. Zhao, D.; Yin, Y.; Zhang, M.; Wang, H.; Lu, C.; Yuan, L.; Shi, S. The optical properties of aerosols at the summit of mount Tai in May and June and the retrieval of the complex refractive index. *Atmosphere* **2020**, *11*, 655. [CrossRef]

Disclaimer/Publisher's Note: The statements, opinions and data contained in all publications are solely those of the individual author(s) and contributor(s) and not of MDPI and/or the editor(s). MDPI and/or the editor(s) disclaim responsibility for any injury to people or property resulting from any ideas, methods, instructions or products referred to in the content.